Biodistribution and Radiation Dosimetry of Deuterium-Substituted ^{18}F-Fluoromethyl-[1, 2-$^{2}H_4$]Choline in Healthy Volunteers

Amarnath Challapalli[1], Rohini Sharma[2], William A. Hallett[3], Kasia Kozlowski[1], Laurence Carroll[1], Diana Brickute[1], Frazer Twyman[1], Adil Al-Nahhas[4], and Eric O. Aboagye[1]

[1]*Department of Surgery and Cancer, Imperial College London, London, United Kingdom;* [2]*Department of Experimental Medicine, Imperial College London, London, United Kingdom;* [3]*Imanova Centre for Imaging Sciences, London, United Kingdom; and* [4]*Department of Radiology/Nuclear Medicine, Imperial College Healthcare NHS Trust, London, United Kingdom*

^{11}C-choline and ^{18}F-fluoromethylcholine (^{18}F-FCH) have been used in patients to study tumor metabolic activity in vivo; however, both radiotracers are readily oxidized to respective betaine analogs, with metabolites detectable in plasma soon after injection of the radiotracer. A more metabolically stable FCH analog, ^{18}F-fluoromethyl-[1,2-$^{2}H_4$]choline (^{18}F-D4-FCH), based on the deuterium isotope effect, has been developed. We report the safety, biodistribution, and internal radiation dosimetry profiles of ^{18}F-D4-FCH in 8 healthy human volunteers. **Methods:** ^{18}F-D4-FCH was intravenously administered as a bolus injection (mean ± SD, 161 ± 2.17 MBq; range, 156–163 MBq) to 8 healthy volunteers (4 men, 4 women). Whole-body (vertex to mid thigh) PET/CT scans were acquired at 6 time points, up to 4 h after tracer injection. Serial whole-blood, plasma, and urine samples were collected for radioactivity measurement and plasma radiotracer metabolites. Tissue ^{18}F radioactivities were determined from quantitative analysis of the images, and time–activity curves were generated. The total numbers of disintegrations in each organ normalized to injected activity (residence times) were calculated as the area under the curve of the time–activity curve normalized to injected activities and standard organ volumes. Dosimetry calculations were performed using OLINDA/EXM 1.1. **Results:** The injection of ^{18}F-D4-FCH was well tolerated in all subjects, with no radiotracer-related serious adverse event reported. The mean effective dose averaged over both men and women (±SD) was estimated to be 0.025 ± 0.004 (men, 0.022 ± 0.002; women, 0.027 ± 0.002) mSv/MBq. The 5 organs receiving the highest absorbed dose (mGy/MBq) were the kidneys (0.106 ± 0.03), liver (0.094 ± 0.03), pancreas (0.066 ± 0.01), urinary bladder wall (0.047 ± 0.02), and adrenals (0.046 ± 0.01). Elimination was through the renal and hepatic systems. **Conclusion:** ^{18}F-D4-FCH is a safe PET radiotracer with a dosimetry profile comparable to other common ^{18}F PET tracers. These data support the further development of ^{18}F-D4-FCH for clinical imaging of choline metabolism.

Key Words: ^{18}F-D4-FCH; biodistribution; dosimetry

J Nucl Med 2014; 55:256–263
DOI: 10.2967/jnumed.113.129577

Choline is a naturally existing substrate in the body that is transported intracellularly and is phosphorylated by the enzyme choline kinase (ChKα) within cells to phosphocholine. Phosphocholine is elevated in several cancers and is a precursor for membrane phosphatidylcholine (*1–4*). Overexpression of ChKα and increased enzyme activity have been reported in prostate, breast, lung, ovarian, and colon cancers (*5,6*) and are largely responsible for the increased phosphocholine levels with malignant transformation and progression (*1*). ^{11}C-choline has been widely used to study tumor metabolic activity in vivo (*7,8*).

The short physical half-life of ^{11}C in ^{11}C-choline (20.4 min) is, however, disadvantageous for routine clinical use. As a result, ^{18}F-labeled choline analogs were developed to overcome this limitation (Fig. 1). The longer half-life of ^{18}F (109.8 min) is potentially advantageous in permitting the late imaging of tumors when sufficient clearance of the parent tracer in systemic circulation has occurred. Since ^{18}F-fluoromethylcholine (^{18}F-FCH) was first developed by DeGrado et al. in 2001 (*9*), it has been extensively used in patients with no reported adverse effects.

^{11}C-choline (and fluoro-analog) is, however, readily oxidized to ^{11}C-betaine by choline oxidase mainly in kidney and liver tissues, with metabolites detectable in plasma soon after injection of the radiotracer (*10–12*). This makes discrimination of the relative contributions of parent radiotracer from catabolites difficult when a late imaging protocol is used. A more metabolically stable FCH analog, ^{18}F-fluoromethyl-[1,2-$^{2}H_4$]choline (^{18}F-D4-FCH), based on the deuterium isotope effect (*13*), has been developed (Fig. 1). The simple substitution of deuterium (^{2}D) for hydrogen (^{1}H) and the presence of ^{18}F improve the stability of the compound and reduce degradation of the parent tracer (*12,14,15*). This modification is hypothesized to increase the net availability of the parent tracer for phosphorylation and trapping within cells, leading to a better signal-to-background contrast, thus improving tumor detection sensitivity of PET.

^{18}F-D4-FCH has been validated for imaging tumors preclinically and was found to be a promising, metabolically stable radiotracer for imaging choline metabolism in tumors (*14,15*). To our knowledge, we present the first human study of ^{18}F-D4-FCH, performed on healthy volunteers, to evaluate the dosimetry, biodistribution, and safety of this radiotracer.

Received Jul. 19, 2013; revision accepted Sep. 16, 2013.
For correspondence or reprints contact: Eric Aboagye, Department of Surgery and Cancer, Imperial College London, Hammersmith Hospital, Du Cane Rd., London W12 0NN, U.K.
E-mail: eric.aboagye@imperial.ac.uk

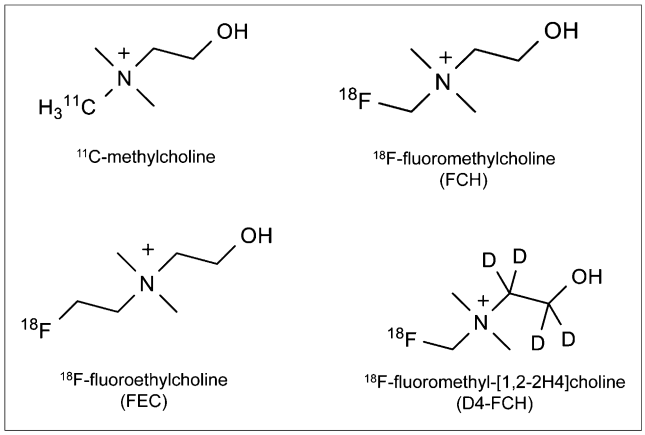

FIGURE 1. Major choline-based tracers in current use and in development.

MATERIALS AND METHODS

Radiopharmaceutical Preparation

^{18}F-D4-FCH was synthesized from the precursor as previously described (*12*). The radiochemical purity of ^{18}F-D4-FCH was 100%, with a specific activity of 48.4 ± 22.8 (mean ± SD; range, 27.3–99.4) GBq/μmol and a pH of 5.5 ± 0.39 (range, 4.84–5.88). The average level of the precursor D4-*N,N*-dimethylaminoethanol (D4-DMAE) used was 2.4 ± 1.52; 0.8–4 μg/mL.

Subjects

Eight healthy volunteers (4 men, 4 women) (mean age ± SD, 62.6 ± 6.12 y; age range, 55–71 y; weight, 65.4 ± 16.6 kg; weight range, 46.2–96.7 kg) were enrolled. Inclusion criteria included age above 50 y, ability to provide informed written consent, and normal medical history (including physical examination, electrocardiogram, hematology, and biochemistry). Exclusion criteria included pregnancy and lactation. Subjects were asked to fast for 4–6 h before tracer injection. Ethical approval for the study was granted by the West-London Research Ethics Committee. All volunteers gave written informed consent to participate in the study, according to the Declaration of Helsinki. The administration of radioactivity was approved by the Administration of Radioactive Substances Advisory Committee, U.K.

Safety, Image Acquisition, Analysis, and Dosimetry

The collection of safety data, image acquisition, image analysis, measurement of blood and urine radioactivity, and the dosimetry calculations were performed as previously described (*16*). Table 1 describes the image acquisition protocol. The mean injected ^{18}F-D4-FCH activity and D4-FCH cold dose in the subjects were 161 ± 2.17 (range, 156–163) MBq and 4.5 ± 1.07 (range, 2–5) μg, respectively.

For each subject and for each source region, the non–decay-corrected ^{18}F activity concentration over the 6 time points (time–activity curve:time–activity curve) was generated. The total number of disintegrations in each organ normalized to injected activity (subsequently referred to as the residence time [τ], kBq·hour/kBq) were calculated as follows (Eq. 1):

$$\tau = \left(\mathrm{AUC} \times V_{organ}\right) / injected\ activity, \qquad \text{Eq. 1}$$

where AUC is the time integral of the non–decay corrected time–activity curve, and V_{organ} is the tabulated organ volume as used in OLINDA/EXM version 1.1 (*17*). For most organs, the AUC included a contribution beyond the scan duration, assuming no further activity redistribution. For the bladder, the measured voided activities were included to form an 8-time-point time–activity curve (Supplemental Fig. 1; supplemental materials are available at http://jnm.snmjournals.org). The bladder time–activity curve was modeled according to Equation 2:

$$A\left(1 - e^{-Bt}\right)e^{-\lambda t} - \sum_i A_i e^{-\lambda(t - t_i)}, \qquad \text{Eq. 2}$$

where *A, B* are fitted parameters, *t* the tracer administration time, λ the decay constant of ^{18}F, and A_i the urine activity voided at time t_i (*18,19*). Across all 8 subjects, the fitted AUCs matched the measured AUCs with a fractional mean difference of 3% and an SD of 7%. The organ-absorbed doses and effective dose (ED) were estimated from the τ for the organs in each subject, provided as input to OLINDA/EXM version 1.1 (*17*).

Metabolite Analysis

Discrete venous blood samples drawn at nominal times of 5, 10, 15, 30, 60, 90, 150, and 240 min after injection were centrifuged at approximately 8,000*g* for 3 min at 4°C to obtain plasma. Plasma metabolite analysis was performed, and samples were clarified by

TABLE 1
Image Acquisition Protocol

Scan	Field of view	No. of bed positions	Minutes per bed position
Attenuation CT1*	Vertex to mid thigh	6–7	
^{18}F-D4-FCH injection			
Emission scan 1†	Vertex to mid thigh‡	6–7	1
Emission scan 2	Vertex to mid thigh	6–7	2
Emission scan 3	Vertex to mid thigh	6–7	5
Emission scan 4	Vertex to mid thigh	6–7	5
Voiding			
Attenuation CT2*	Vertex to mid thigh	6–7	
Emission scan 5	Vertex to mid thigh	6–7	7
Emission scan 6	Vertex to mid thigh	6–7	7

*CT settings: 130 kV; 15 effective mAs; pitch, 1.5; slice thickness, 5 mm; rotation time, 0.6 s; and effective dose, 2.5 mSv.
†Emission data were reconstructed using ordered-subsets expectation maximization algorithm (3 iterations and 21 subsets).
‡Imaging performed caudocranially.

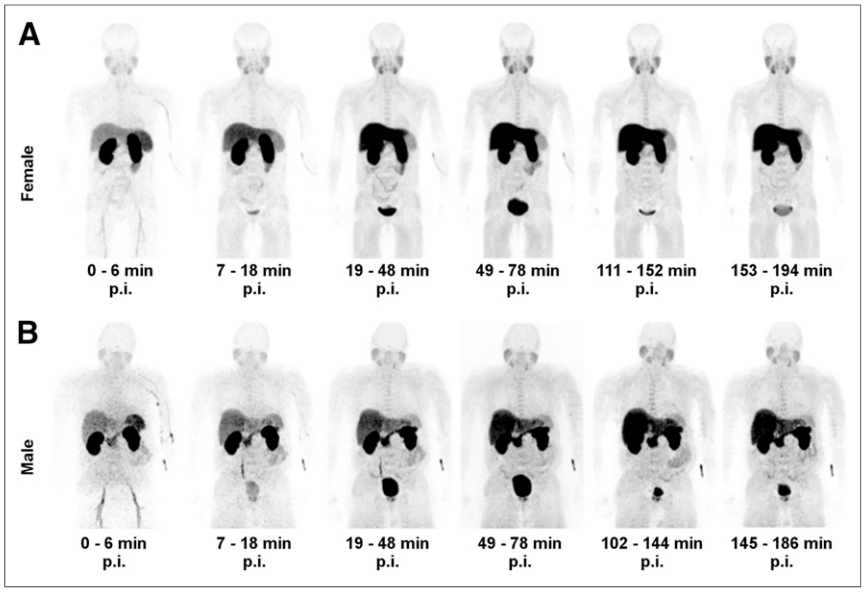

FIGURE 2. Series of whole-body maximum-intensity-projection images of representative female (A) and male (B) subjects showing biodistribution of ^{18}F activity after tracer injection up to 194 min after injection (p.i.) of ^{18}F-D4-FCH. Incidental increased uptake of radiotracer noted in prostate of male subject was secondary to benign prostatic hyperplasia. Apparent delayed uptake in liver of male subject was not present in other male subjects.

protein precipitation (*12*). All samples were instantly processed for analysis by high-performance liquid chromatography (HPLC) (1200 series system; Agilent). A guard column (Bondapak-C18, 10 μm,125A; Waters) and an analytic column (Luna-SCX, 240 × 4.6 mm,10 μm; Phenomenex) were used. Briefly, ice-cold acetonitrile (3.75–12 mL) was added to plasma samples (0.5–2.0 mL). The resulting suspension was centrifuged (15,490*g*, 4°C, 3 min). The supernatant was then decanted and evaporated to dryness on an evaporator under vacuum (at 40°C) and then resuspended in HPLC mobile phase (1.1 mL) and filtered through a syringe filter (0.2 μm) to remove particulates. The mobile phase comprised 0.25 M sodium dihydrogen phosphate (pH 4.8) and acetonitrile (9:1 v/v) delivered at a flow rate of 2 mL/min and a total run time of 10 min. Thirty fractions were collected over the course of the analysis, and radioactivity was measured using a PerkinElmer-Wizard-1470 automated γ counter.

RESULTS

Safety

^{18}F-D4-FCH was found to be safe and well tolerated in all subjects. No tracer-related serious adverse events or adverse events were observed in relation to ^{18}F-D4-FCH injection. No significant changes in vital signs, clinical laboratory blood tests, or electrocardiograms were observed.

Biodistribution

After the administration of ^{18}F-D4-FCH, radioactivity was initially detected in the vascular compartment and then rapidly distributed to the liver, kidneys, pancreas, and spleen. About 7% of the injected activity (decay-corrected to injection time) was eliminated within the first 4 h through the kidneys (6% after 2 h). Radioactivity was already detectable in the urinary bladder at about 7 min after tracer administration. The initial radioactivity uptake in the liver gradually increased with time after tracer injection. Increased uptake was also noted in the pituitary, salivary glands, and bone marrow. Typical images illustrating tracer uptake at various time points from a representative female and male subject are shown in Figure 2. There were no differences in biodistribution profiles between men and women. Time–activity curves were generated for various organs (Fig. 3). The mean τ for male and female subjects are summarized in Table 2. The τ contribution from the extrapolated part of AUC beyond the last time point for imaging accounted for 38% of the total τ, contributing to 61% of the total ED.

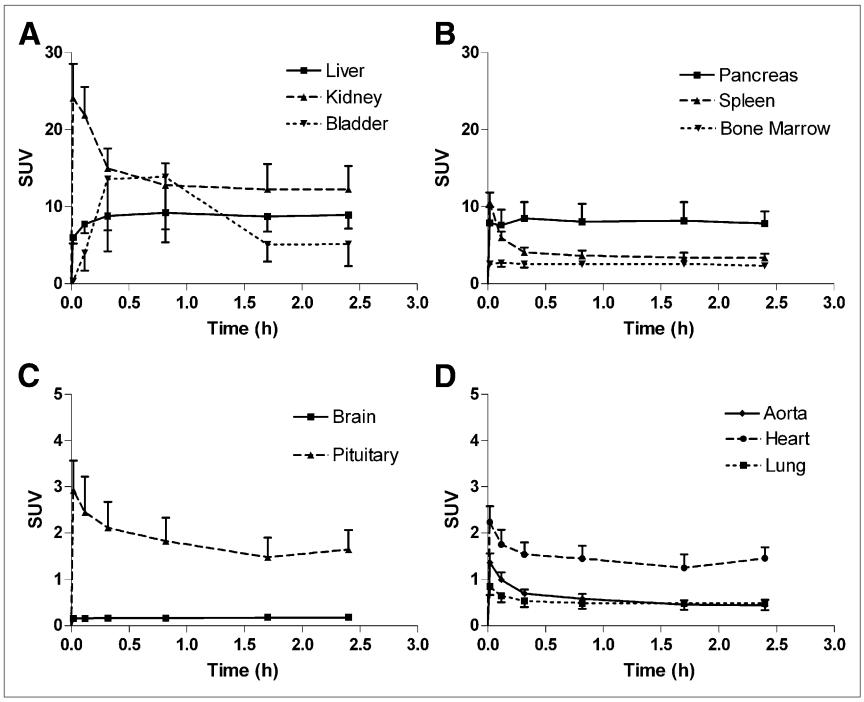

FIGURE 3. Mean decay-corrected time–activity curves normalized to injected activity (kBq) and body weight (g) for ^{18}F-D4-FCH. Time–activity curves were generated for several organs at various time points up to 4 h after tracer administration in elimination organs (liver, kidney, and urinary bladder) (A); pancreas, spleen, and bone marrow (B); cranium (C); and thorax (D). Error bars represent 1 SD from mean and are shown 1-sided for clarity. SUV = standardized uptake value.

Dosimetry

Table 3 summarizes the mean organ-absorbed dose estimates for ^{18}F-D4-FCH injection. The mean effective dose averaged over both men and women was estimated to be 0.025 ± 0.004 (men, 0.022 ± 0.002;

TABLE 2
Mean Residence Times (τ) of ^{18}F-D4-FCH for Different Organs in Male (n = 4) and Female (n = 4) Volunteers

	τ (kBq·h/kBq)			
	Men		Women	
Organ	Mean	SD	Mean	SD
Adrenal	0.003	0.001	0.003	0.001
Brain	0.009	0.001	0.012	0.003
Breast			0.005	0.001
Gallbladder	0.005	0.001	0.006	0.006
Heart contents	0.009	0.003	0.009	0.001
Heart wall	0.017	0.004	0.017	0.001
Kidney	0.126	0.043	0.170	0.046
Liver	0.534	0.138	0.681	0.097
Lower large intestine	0.008	0.003	0.007	0.003
Lung	0.061	0.009	0.042	0.006
Muscle	1.036	0.381	0.873	0.191
Ovaries*			0.00004	0.00008
Pancreas	0.027	0.002	0.025	0.006
Red marrow	0.102	0.018	0.125	0.013
Small intestine	0.071	0.015	0.108	0.033
Spleen	0.022	0.002	0.026	0.002
Stomach wall	0.027	0.008	0.022	0.012
Testis	0.001	0.000		
Thymus	0.00047	0.00015	0.00164	0.00038
Thyroid	0.001	0.000	0.001	0.000
Upper large intestine	0.010	0.001	0.013	0.001
Urinary bladder†	0.059	0.027	0.075	0.025
Uterus			0.004	0.003
Remainder	0.511	0.450	0.414	0.076

*In 3 subjects, ovaries were not visible due to postmenopausal atrophy.
†Urinary bladder τ is for 2-h voiding scenario.

women, 0.027 ± 0.002) mSv/MBq. The 5 organs receiving the highest absorbed dose (mGy/MBq), averaged over both men and women, were the kidneys (0.106 ± 0.03), liver (0.094 ± 0.03), pancreas (0.066 ± 0.01), urinary bladder wall (0.047 ± 0.02), and adrenals (0.046 ± 0.01). The values quoted are based on the 2-h bladder-voiding scenario. This is likely to be conservative in routine imaging scenarios in which subjects would be encouraged to consume moderate quantities of fluids and empty their bladders regularly as is done for ^{18}F-FDG studies. If the 4-h voiding scenario were used, this would increase the bladder wall absorbed dose by 59% (increase of 0.027 mGy/MBq: averaged for men and women).

Metabolism of ^{18}F-D4-FCH

The metabolism of ^{18}F-D4-FCH in plasma at discrete time points after tracer injection was evaluated using HPLC. Typical high-performance liquid chromatograms of ^{18}F-D4-FCH and its metabolite in the plasma at various time points after tracer injection are shown in Figure 4. ^{18}F-D4-FCH eluted at approximately 6 min and ^{18}F-D4-betaine at 3 min. ^{18}F-D4-betaine was detected as early as 10 min after injection. The chromatogram of ^{18}F-D4-FCH and its metabolite in urine (Supplemental Fig. 2) shows elimination of ^{18}F-D4-betaine predominantly. The ^{18}F-D4-FCH parent fraction (fraction of radioactivity in blood remaining as ^{18}F-D4-FCH) and the whole blood–to–plasma ratio of radioactivity are shown in Figure 5. At about 3.5 h after tracer injection, 31% of radioactivity remained as parent ^{18}F-D4-FCH in circulation. The ratio of radioactivity in blood to that in plasma approximated unity, over the time course of the study.

DISCUSSION

We have shown in this first-in-human study that the deuterium-substituted FCH analog, ^{18}F-D4-FCH, is safe and well tolerated. Aberrant phospholipid metabolism of cancers (*5*), associated with upregulation of ChKα, a biomarker of malignant transformation (*1*), has been studied using proton and phosphorous MR spectroscopy (MRS) of tumor tissue biopsies and noninvasive tissue measurements (*20*). The inherently poor sensitivity of MRS in vivo precludes resolution of individual choline metabolite resonances. PET-labeled choline tracers provide improved sensitivity when compared with MRS and enable dynamic measurements of the early steps of choline metabolism to be assessed by virtue of cellular radiotracer trapping but without the chemical resolution of ex vivo MRS. To date, ^{11}C-choline and ^{18}F-FCH have been extensively used for the clinical imaging of prostate, brain, breast, and esophageal carcinomas (*7,8*). Because of the metabolic instability of choline radiotracers and the desire to use late imaging protocols (~60 min, to permit elimination of nonspecific metabolites), we developed a more stable choline radiotracer, ^{18}F-D4-FCH (*12*). A series of preclinical studies showed that the new tracer has improved protection against oxidation by choline oxidase, the key choline catabolic enzyme, via a ^{1}H/^{2}D isotope effect, together with fluorine substitution (*12,14,15*). The objective of this

TABLE 3
Mean Organ-Absorbed Dose Estimates Expressed in mGy/MBq for ^{18}F-D4-FCH (n = 8) with Bladder-Voiding Scenarios

Organ	Mean absorbed dose estimates (mGy/MBq)			
	2-h bladder-voiding scenario		4-h bladder-voiding scenario	
	Mean	SD	Mean	SD
Adrenals	0.046	0.011	0.046	0.011
Brain	0.004	0.001	0.004	0.001
Breasts	0.007	0.001	0.007	0.001
Gallbladder wall	0.034	0.009	0.033	0.009
Lower large intestine wall	0.015	0.002	0.015	0.002
Small intestine	0.031	0.009	0.031	0.009
Stomach wall	0.040	0.010	0.040	0.010
Upper large intestine wall	0.019	0.003	0.019	0.003
Heart wall	0.023	0.004	0.023	0.004
Kidneys	0.106	0.034	0.106	0.033
Liver	0.093	0.028	0.093	0.029
Lungs	0.019	0.002	0.019	0.002
Muscle	0.014	0.003	0.014	0.003
Ovaries	0.013	0.002	0.013	0.002
Pancreas	0.066	0.009	0.066	0.008
Red marrow	0.017	0.001	0.017	0.001
Osteogenic cells	0.015	0.002	0.014	0.002
Skin	0.005	0.001	0.005	0.001
Spleen	0.038	0.007	0.038	0.007
Testes	0.010	0.002	0.010	0.002
Thymus	0.015	0.006	0.015	0.006
Thyroid	0.017	0.003	0.017	0.003
Urinary bladder wall	0.046	0.018	0.074	0.030
Uterus	0.017	0.006	0.018	0.006
Total body	0.014	0.002	0.014	0.002
Mean ED (mSv/MBq)	0.025	0.004	0.027	0.004

study was to investigate the biodistribution and dosimetry in human subjects and extend pharmacokinetic aspects of the preclinical findings into human application.

The early tissue distribution of ^{18}F-D4-FCH was not dissimilar from that of ^{18}F-FCH reported by DeGrado et al. (*21*), though their study evaluated the distribution and dosimetry over a period of up to 1 h only. Injection of ^{18}F-D4-FCH led to rapid washout of the ^{18}F activity from the vascular compartment, and elimination was primarily via the renal and hepatic routes. Renal excretion (7% in 4 h) was relatively lower than for routinely used radiotracers such as ^{18}F-FDG (21% in 2 h) (*22,23*) and similar to that of the other choline analogs (Supplemental Table 1). We determined the mean ED of ^{18}F-D4-FCH as 0.025 mSv/MBq, which is comparable with the ED of ^{18}F-FDG (0.019 mSv/MBq) (*22*). The dose limits specified in the Code of Federal Regulations (USA) per single administration of a radioactive drug for research purposes are 30 mSv to the whole body, blood-forming organs, lens of the eye, and gonads, with a maximum annual dose of 50 mSv. The maximum-allowable single and annual doses to all other organs are 50 and 150 mSv, respectively (*24*). If we assume a 370-MBq administered radioactivity for ^{18}F-D4-FCH (typical of many PET tracers), the ED would be 9.3 mSv. For this administered radioactivity level, the equivalent dose received by the gonads would be estimated as 1.9 mSv. These are well within the dose limits specified above.

As indicated above, both transport and phosphorylation by ChKα are putative mechanisms for radiotracer localization. Examination of ^{18}F-D4-FCH localization in brain tissue was low, with the pituitary being the only organ of the brain showing a high uptake (Fig. 3C). This is in keeping with previous reports of radiolabeled choline (*25,26*). The brain has a limited capacity to synthesize choline de novo. Thus, most choline enters the brain from the circulation through saturable transport at the blood–brain barrier (*27*) or through the high-affinity choline transporters, which are highly expressed in the neural tissues (*28*). The lack of significant radiotracer localization in healthy brain in some ways leads us to speculate that the rate-limiting step for ^{18}F-D4-FCH tissue localization in humans is phosphorylation by ChKα rather than transport. The higher uptake in the pituitary gland noted in this study and in the report of Mertens et al. (*26*) could be due to this gland being situated outside the blood–brain barrier. This is in contrast to that reported by Schillaci et al., who documented physiologic uptake in the pituitary in only 1 of the 80 subjects evaluated (*29*). Physiologic accumulation of ^{18}F-D4-FCH was also seen in the salivary glands and pancreas as reported previously (*26,30*). However, the mechanism of uptake is unclear. It has been suggested that uptake in the pancreas could be due to the incorporation of radiolabeled choline into phosphatidylcholine and lysophosphatidylcholine, which are in abundance in the pancreatic exocrine secretions (*30*).

There is paucity of plasma metabolism information on ^{18}F-choline analogs in humans. In translating our finding from preclinical validation to patients, we hypothesized that the slower metabolism of choline tracers in humans than rodents (*10,11*) will result in

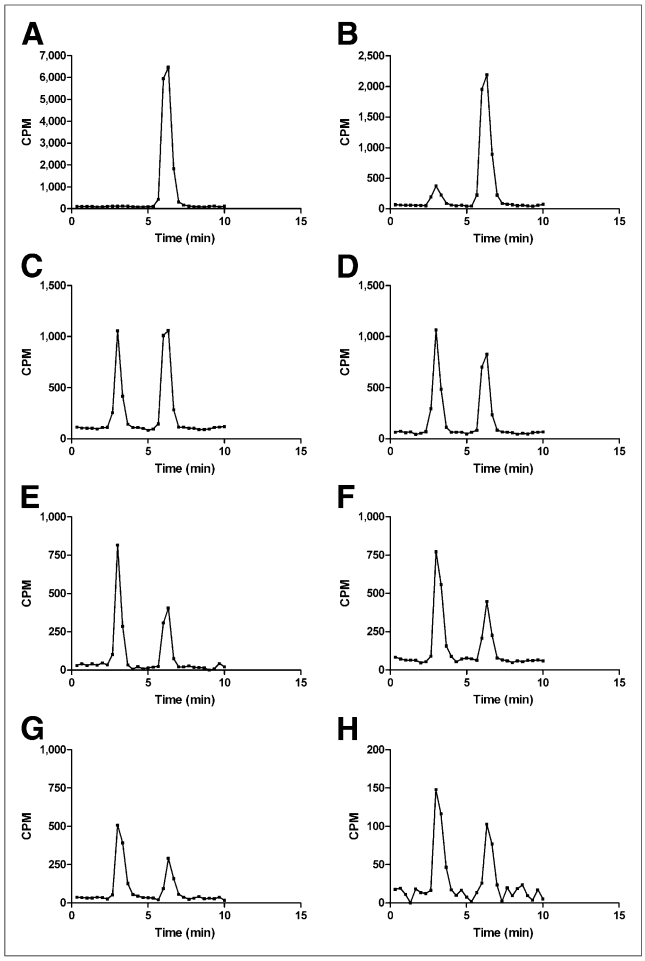

FIGURE 4. Typical high-performance liquid chromatogram of ^{18}F-D4-FCH and its metabolite ^{18}F-D4-betaine in plasma. Analysis of metabolism of ^{18}F-D4-FCH at 2.5 (A), 10 (B), 20 (C), 30 (D), 60 (E), 90 (F), 150 (G), and 240 (H) min after tracer injection shows detection of ^{18}F-D4-betaine as early as 10 min, a proportion of which increases with time. *y*-axis scale is different due to decrease in counts per minute (CPM).

relatively slow metabolism of ^{18}F-D4-FCH to ^{18}F-D4-betaine, compared with published studies for ^{11}C-choline (*31–33*). In support of this hypothesis, there was 38% of parent ^{18}F-D4-FCH in plasma at 60 min, decreasing to 31% at 4 h. This represents an improvement in metabolic stability for choline tracers in use clinically; for example, a 2-fold higher metabolic stability is observed for ^{18}F-D4-FCH relative to published data for ^{11}C-choline by our team (Fig. 6A). The metabolic stability of ^{18}F-D4-FCH observed was not due to a high total cold compounds in the radiopharmaceutical, which may negatively impact on clearance. In contrast, the dose solution had higher specific activity (48.4 GBq/μmol) and pseudospecific activity (relative to the precursor D4-DMAE) than previously reported for ^{11}C-choline (*34*), the upper quality control release limit with respect to precursor being set at 10 μg (at least 10- to 20-fold lower). The lower levels of the precursor D4-DMAE along with the high specific activity are an added theoretic advantage, because DMAE is known to modulate the transport and phosphorylation of radiolabeled choline (*35*). The lower concentration of DMAE is also known to enhance the visualization of the tumors (*36*). The role of specific activity on ^{18}F-D4-FCH tumor uptake requires further evaluation.

In keeping with the preclinical studies (*12,14,15*), localization of the ^{18}F-D4-FCH was most pronounced in the kidneys and liver. Radiotracer uptake in kidneys and liver is likely to represent phosphorylation by ChKα, with minor oxidation of ^{18}F-D4-FCH to ^{18}F-D4-betaine (*14,15*). Comparison of the early phase (0–60 min) biodistribution profiles of ^{18}F-D4-FCH and ^{11}C-choline showed lower liver radioactivity and higher kidney and bladder radioactivities for ^{18}F-D4-FCH (Figs. 6B–6D). The differences in radiotracer distribution kinetics are likely due to the preponderance of phosphorylation over oxidation (*15*). The higher activity of ^{18}F-D4-FCH in the bladder (enhanced urinary clearance; Fig. 6D) and the predominance of ^{18}F-D4-betaine in the excreted urine chromatograms (Supplemental Fig. 2) suggest incomplete tubular reabsorption of the parent tracer, similar to that seen with ^{18}F-FCH (*9*). This is in contrast to the efficient tubular reabsorption of the nature-identical ^{11}C-betaine (*37*).

Given the low background uptake of ^{18}F-D4-FCH in the thorax and brain, we envisage that this radiotracer will find utility in the following clinical scenarios: as a prognostic marker in lung cancer, supported by the observation that overexpression of Chkα predicts for patient survival in lung cancer (*6*), and in the detection of primary and recurrent brain tumors, supported by MRS imaging studies (*38*). The use of ^{18}F-D4-FCH in prostate cancer including

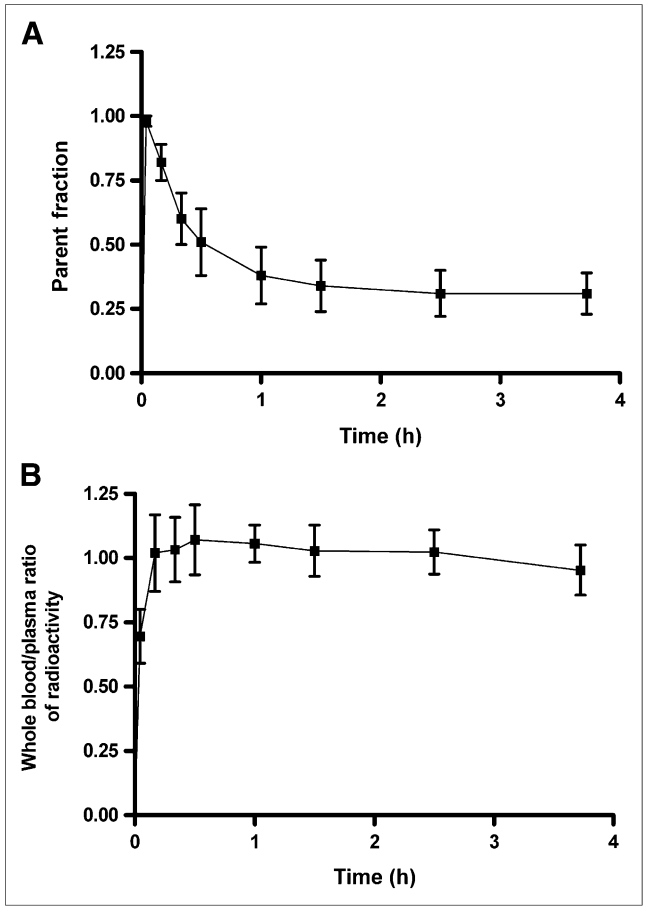

FIGURE 5. Time course of in vivo oxidation of ^{18}F-D4-FCH (A) and ratio of whole blood to plasma radioactivity (B). Thirty-one percent of radioactivity remains as parent ^{18}F-D4-FCH in circulation at about 3.5 h after tracer injection. Ratio of radioactivity in blood to that in plasma was close to unity.

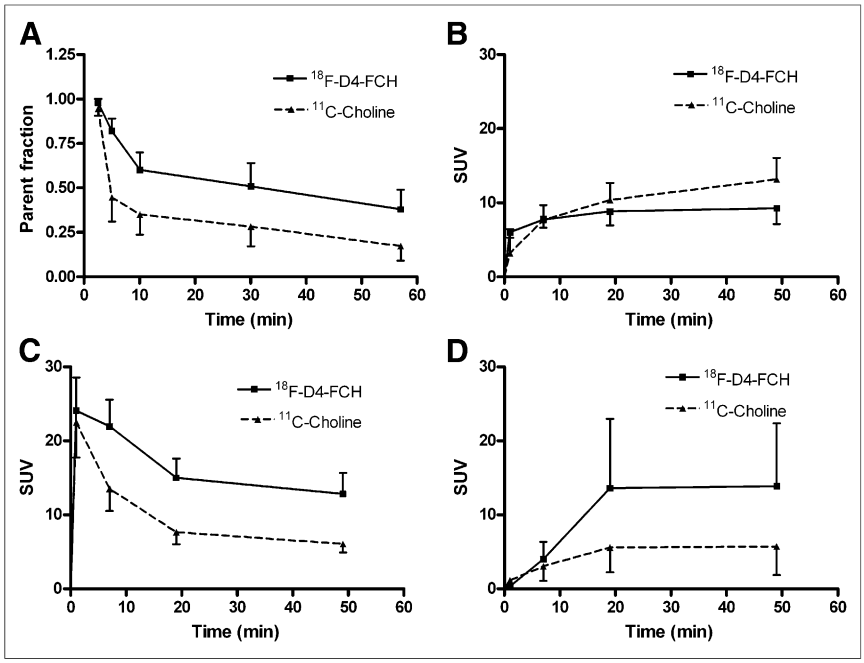

FIGURE 6. Time–activity curves of ^{18}F-D4-FCH liver, kidney, and bladder and comparison with ^{11}C-choline in breast and prostate cancer patients (primary data, excluding metabolites and normal-tissue uptake, were published in Contractor et al. (*33*) and Contractor et al. (*31*)). (A) Comparison of parent radiotracer fraction over 1 h after tracer injection. Thirty-eight percent of parent ^{18}F-D4-FCH remains in circulation, compared with 17% of parent ^{11}C-choline in breast (mean injected activity, 320 MBq) patient cohort. Mean decay-corrected and normalized radioactivity levels for ^{18}F-D4-FCH and ^{11}C-choline in: liver (B), kidney (C), and bladder (D). Key difference between two ^{11}C-choline studies relates to approximately 10-fold higher levels of unlabeled choline and dimethylaminoethanol precursor (^{11}C-choline synthesized as per Pascali et al. (*34*)). ^{18}F-D4-FCH dose solution has extremely low levels of both precursor and unlabeled cold material, that is, high specific radioactivity. ^{11}C-choline metabolite analysis was performed as described in Contractor et al. (*32*).

localized and advanced disease remains to be determined. In this regard, the urinary excretion of ^{18}F-D4-FCH, although lower than ^{18}F-FDG, for example, may still obscure detection. Furthermore, it should be noted that patients fasted in this study; thus, the impact of postprandial bowel uptake needs further clarification.

In summary, ^{18}F-D4-FCH injection is safe and well tolerated, with a favorable dosimetry profile in healthy volunteers. Organ dose estimates are similar to those seen with other routine ^{18}F-labeled tracers. The potential risks due to radiation are within accepted limits. The radiotracer was relatively stable in vivo. Further clinical studies are now warranted to evaluate the utility of ^{18}F-D4-FCH in cancer patients.

CONCLUSION

^{18}F-D4-FCH is a safe PET tracer, with a favorable radiation dosimetry profile for clinical imaging. The effective dose is 0.025 ± 0.004 mSv/MBq, which is within the range of other common ^{18}F PET tracers.

DISCLOSURE

The costs of publication of this article were defrayed in part by the payment of page charges. Therefore, and solely to indicate this fact, this article is hereby marked "advertisement" in accordance with 18 USC section 1734. The study was supported by the U.K. Medical Research Council (MRC) grant MC-A652-5PY80; Joint Cancer Research U.K. and Engineering and Physical Sciences Research Council Cancer Imaging Centre at Imperial College London, in association with the MRC and Department of Health (England) grant C2536/A10337; Experimental Cancer Medicine Centers grant C37/A7283; and the National Institute for Health Research (NIHR) Biomedical Research Centre award to Imperial College Healthcare NHS Trust and Imperial College London. No other potential conflict of interest relevant to this article was reported.

ACKNOWLEDGMENTS

We thank the healthy volunteers, staff of Imanova Ltd., and staff of NIHR/Wellcome Trust Imperial Clinical Research Facility for their support of the trial.

REFERENCES

1. Aboagye EO, Bhujwalla ZM. Malignant transformation alters membrane choline phospholipid metabolism of human mammary epithelial cells. *Cancer Res.* 1999;59:80–84.
2. Exton JH. Phosphatidylcholine breakdown and signal transduction. *Biochim Biophys Acta.* 1994;1212:26–42.
3. George TP, Morash SC, Cook HW, Byers DM, Palmer FB, Spence MW. Phosphatidylcholine biosynthesis in cultured glioma cells: evidence for channeling of intermediates. *Biochim Biophys Acta.* 1989;1004:283–291.
4. Teegarden D, Taparowsky EJ, Kent C. Altered phosphatidylcholine metabolism in C3H10T1/2 cells transfected with the Harvey-ras oncogene. *J Biol Chem.* 1990;265:6042–6047.
5. Ramírez de Molina A, Rodriguez-Gonzalez A, Gutierrez R, et al. Overexpression of choline kinase is a frequent feature in human tumor-derived cell lines and in lung, prostate, and colorectal human cancers. *Biochem Biophys Res Commun.* 2002;296:580–583.
6. Ramírez de Molina A, Sarmentero-Estrada J, Belda-Iniesta C, et al. Expression of choline kinase alpha to predict outcome in patients with early-stage non-small-cell lung cancer: a retrospective study. *Lancet Oncol.* 2007;8:889–897.
7. Treglia G, Giovannini E, Di Franco D, et al. The role of positron emission tomography using carbon-11 and fluorine-18 choline in tumors other than prostate cancer: a systematic review. *Ann Nucl Med.* 2012;26:451–461.
8. Umbehr MH, Muntener M, Hany T, Sulser T, Bachmann LM. The role of ^{11}C-choline and ^{18}F-fluorocholine positron emission tomography (PET) and PET/CT in prostate cancer: a systematic review and meta-analysis. *Eur Urol.* 2013;64:106–117.
9. DeGrado TR, Coleman RE, Wang S, et al. Synthesis and evaluation of ^{18}F-labeled choline as an oncologic tracer for positron emission tomography: initial findings in prostate cancer. *Cancer Res.* 2001;61:110–117.
10. Bansal A, Shuyan W, Hara T, Harris RA, Degrado TR. Biodisposition and metabolism of [^{18}F]fluorocholine in 9L glioma cells and 9L glioma-bearing fisher rats. *Eur J Nucl Med Mol Imaging.* 2008;35:1192–1203.
11. Roivainen A, Forsback S, Gronroos T, et al. Blood metabolism of [methyl-^{11}C] choline; implications for in vivo imaging with positron emission tomography. *Eur J Nucl Med.* 2000;27:25–32.
12. Smith G, Zhao Y, Leyton J, et al. Radiosynthesis and pre-clinical evaluation of [^{18}F]fluoro-[1,2-(2)H(4)]choline. *Nucl Med Biol.* 2011;38:39–51.
13. Gadda G. pH and deuterium kinetic isotope effects studies on the oxidation of choline to betaine-aldehyde catalyzed by choline oxidase. *Biochim Biophys Acta.* 2003;1650:4–9.
14. Leyton J, Smith G, Zhao Y, et al. [^{18}F]fluoromethyl-[1,2-2H4]-choline: a novel radiotracer for imaging choline metabolism in tumors by positron emission tomography. *Cancer Res.* 2009;69:7721–7728.

15. Witney TH, Alam IS, Turton DR, et al. Evaluation of deuterated ^{18}F- and ^{11}C-labeled choline analogs for cancer detection by positron emission tomography. *Clin Cancer Res.* 2012;18:1063–1072.
16. Challapalli A, Kenny LM, Hallett WA, et al. ^{18}F-ICMT-11, a caspase-3-specific PET tracer for apoptosis: biodistribution and radiation dosimetry. *J Nucl Med.* 2013;54:1551–1556.
17. Stabin MG, Sparks RB, Crowe E. OLINDA/EXM: the second-generation personal computer software for internal dose assessment in nuclear medicine. *J Nucl Med.* 2005;46:1023–1027.
18. Graham MM, Peterson LM, Link JM, et al. Fluorine-18-fluoromisonidazole radiation dosimetry in imaging studies. *J Nucl Med.* 1997;38:1631–1636.
19. Thomas SR, Stabin MG, Chen CT, Samaratunga RC. MIRD pamphlet no. 14 revised: a dynamic urinary bladder model for radiation dose calculations. Task Group of the MIRD Committee, Society of Nuclear Medicine. *J Nucl Med.* 1999;40:102S–123S.
20. Glunde K, Bhujwalla ZM. Metabolic tumor imaging using magnetic resonance spectroscopy. *Semin Oncol.* 2011;38:26–41.
21. DeGrado TR, Reiman RE, Price DT, Wang S, Coleman RE. Pharmacokinetics and radiation dosimetry of ^{18}F-fluorocholine. *J Nucl Med.* 2002;43:92–96.
22. Radiation dose to patients from radiopharmaceuticals (addendum 2 to ICRP publication 53). ICRP Publication 80. *Ann ICRP.* 1998;28:1–126.
23. Jones SC, Alavi A, Christman D, Montanez I, Wolf AP, Reivich M. The radiation dosimetry of 2 [F-18]fluoro-2-deoxy-D-glucose in man. *J Nucl Med.* 1982;23:613–617.
24. Radioactive drugs for certain research uses. Code of Federal Regulations Title 21, Part 361.1. http://www.accessdata.fda.gov/scripts/cdrh/cfdocs/cfcfr/CFRSearch.cfm?fr=361. Accessed December 17, 2013.
25. Hara T, Kosaka N, Shinoura N, Kondo T. PET imaging of brain tumor with [methyl-^{11}C]choline. *J Nucl Med.* 1997;38:842–847.
26. Mertens K, Ham H, Deblaere K, et al. Distribution patterns of ^{18}F-labelled fluoromethylcholine in normal structures and tumors of the head: a PET/MRI evaluation. *Clin Nucl Med.* 2012;37:e196–e203.
27. Allen DD, Smith QR. Characterization of the blood-brain barrier choline transporter using the in situ rat brain perfusion technique. *J Neurochem.* 2001;76:1032–1041.
28. Michel V, Yuan Z, Ramsubir S, Bakovic M. Choline transport for phospholipid synthesis. *Exp Biol Med (Maywood).* 2006;231:490–504.
29. Schillaci O, Calabria F, Tavolozza M, et al. ^{18}F-choline PET/CT physiological distribution and pitfalls in image interpretation: experience in 80 patients with prostate cancer. *Nucl Med Commun.* 2010;31:39–45.
30. Hara T, Kosaka N, Kishi H. PET imaging of prostate cancer using carbon-11-choline. *J Nucl Med.* 1998;39:990–995.
31. Contractor K, Challapalli A, Barwick T, et al. Use of [^{11}C]choline PET-CT as a non-invasive method for detecting pelvic lymph node status from prostate cancer and relationship with choline kinase expression. *Clin Cancer Res.* 2011;17:7673–7683.
32. Contractor KB, Kenny LM, Stebbing J, et al. [^{11}C]choline positron emission tomography in estrogen receptor-positive breast cancer. *Clin Cancer Res.* 2009;15:5503–5510.
33. Contractor KB, Kenny LM, Stebbing J, et al. Biological basis of [^{11}C]choline-positron emission tomography in patients with breast cancer: comparison with [^{18}F]fluorothymidine positron emission tomography. *Nucl Med Commun.* 2011;32:997–1004.
34. Claudio Pascali AB, Itawa R, Cambiè M, Bombardieri E. [^{11}C]methylation on a C18 Sep-Pak cartridge: a convenient way to produce [N-methyl-^{11}C]choline. *J Labelled Comp Radiopharm.* 2000;43:195–203.
35. Hara T. ^{18}F-fluorocholine: a new oncologic PET tracer. *J Nucl Med.* 2001;42:1815–1817.
36. Slaets D, De Bruyne S, Dumolyn C, Moerman L, Mertens K, De Vos F. Reduced dimethylaminoethanol in [^{18}F]fluoromethylcholine: an important step towards enhanced tumour visualization. *Eur J Nucl Med Mol Imaging.* 2010;37:2136–2145.
37. Pummer S, Dantzler WH, Lien YH, Moeckel GW, Volker K, Silbernagl S. Reabsorption of betaine in Henle's loops of rat kidney in vivo. *Am J Physiol Renal Physiol.* 2000;278:F434–F439.
38. Horská A, Barker PB. Imaging of brain tumors: MR spectroscopy and metabolic imaging. *Neuroimaging Clin N Am.* 2010;20:293–310.